

Supporting Information

Responsive Assembly of Silver Nanoclusters with Biofilm Locally Amplified Bactericidal Effect to Enhance Treatments Against Multidrug-Resistant Bacterial Infections

Jiahe Wu,^{†,‡,#} Fangyuan Li,^{†,‡,#} Xi Hu,[†] Jingxiong Lu,[†] Xiaolian Sun,[‡] Jianqing Gao,^{*,†} and
Daishun Ling^{*,†,§,‡}

[†]Institute of Pharmaceutics, College of Pharmaceutical Sciences, Zhejiang University, Hangzhou 310058, P. R. China.

[§]Hangzhou Institute of Innovative Medicine, Zhejiang University, Hangzhou 310058, P. R. China

[‡]Key Laboratory of Biomedical Engineering of the Ministry of Education, College of Biomedical Engineering & Instrument Science, Zhejiang University, Hangzhou 310058, P. R. China.

[‡]Department of Pharmaceutical Analysis, China Pharmaceutical University, Nanjing 210009, P. R. China.

[#]These authors contributed equally to this work.

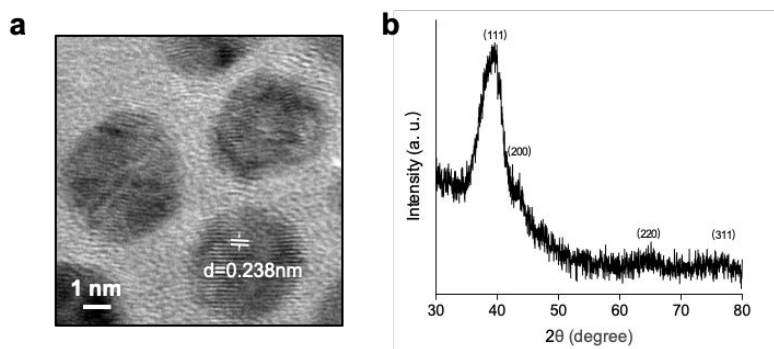


Figure S1. (a) The high-resolution TEM (HRTEM) images of AgNCs. (b) XRD analysis of AgNCs.

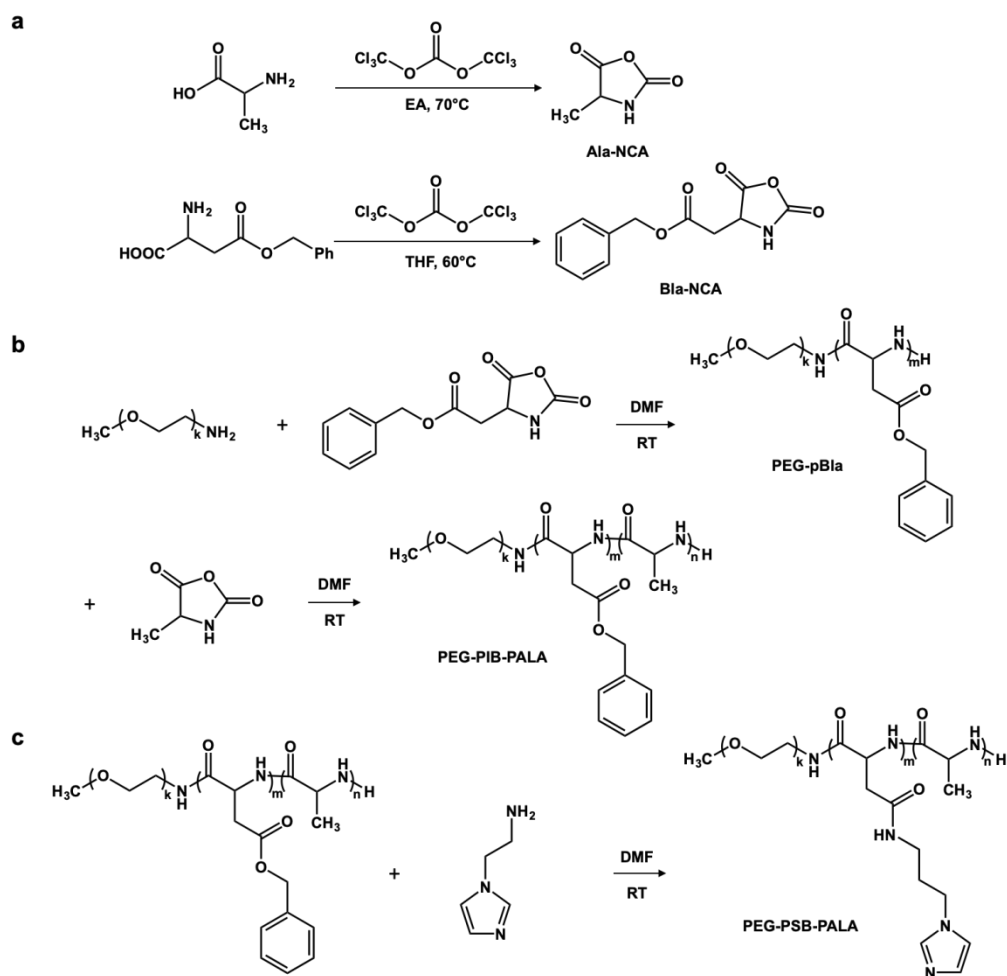


Figure S2. The synthetic route of pH-sensitive polymer (PEG-PSB-PALA). (a) The synthesis of Ala-NCA and Bla-NCA. (b) Ring-opening-polymerization process to obtain the PEG-PIB-PALA. (c) Final product PEG-PSB-PALA was synthesized *via* aminolysis reaction.

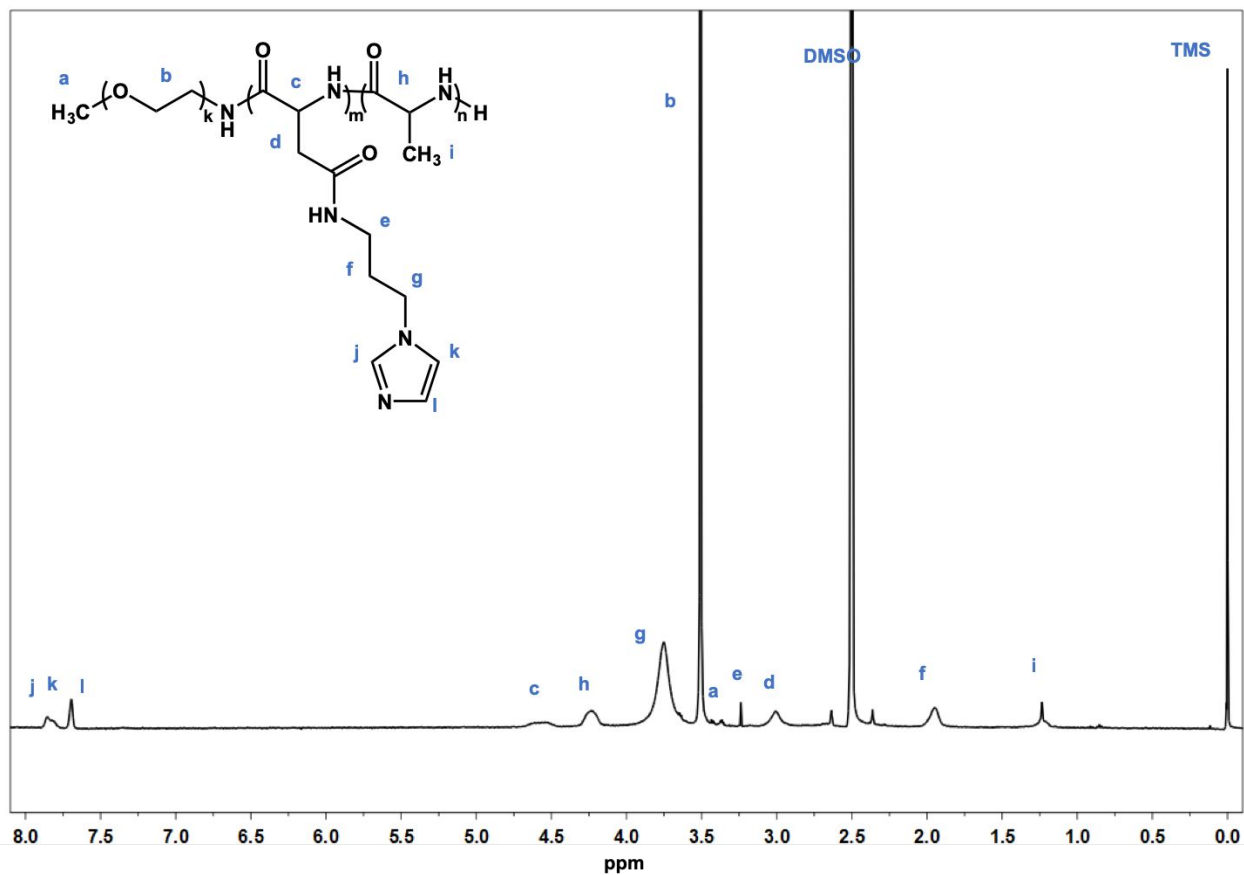


Figure S3. ¹H NMR spectra analysis of PEG-PSB-PALA.

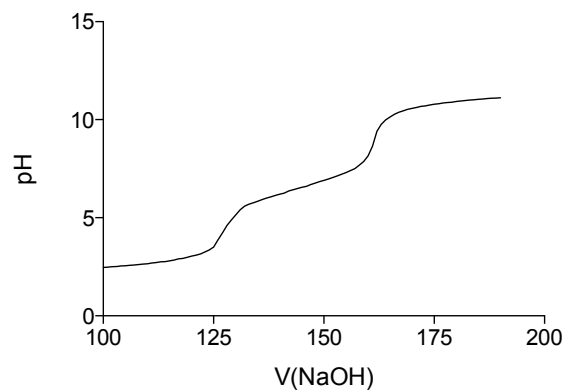


Figure S4. The titration curve of PEG-PSB-PALA titrated by sodium hydroxide solution (1.0 M).

The concentration of PEG-PSB-PALA for titration was 1 mg mL⁻¹.

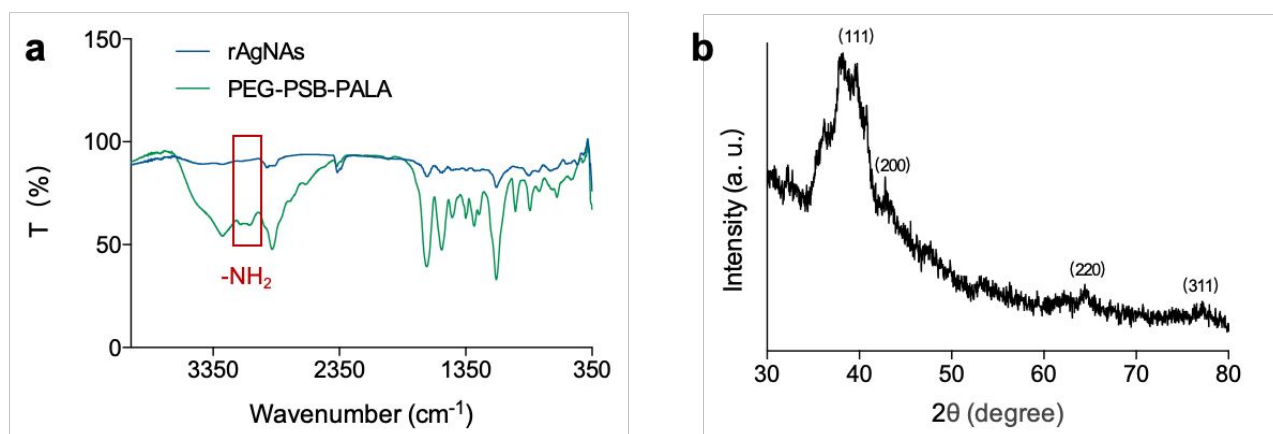


Figure S5. (a) IR spectra of rAgNAs (blue line) and PEG-PSB-PALA (green line). (b) XRD analysis of rAgNAs.

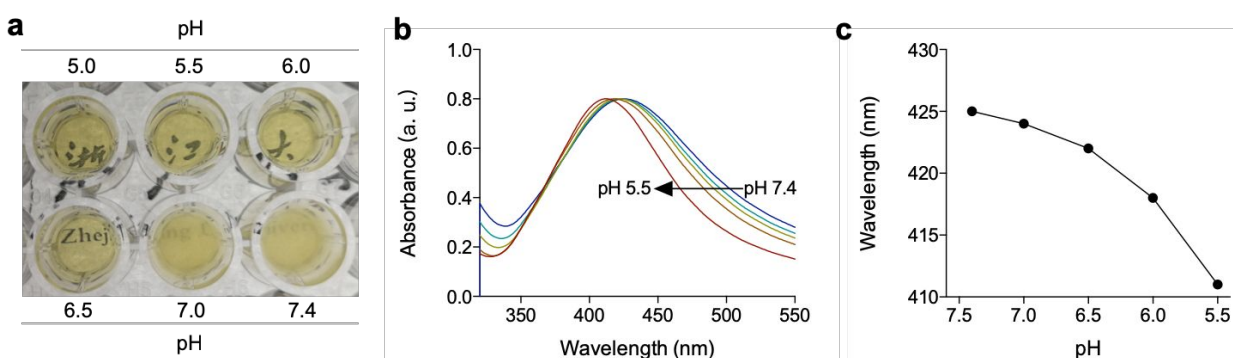


Figure S6. Characterization of the pH-sensitivity of rAgNAs. (a) Appearance of rAgNAs with different pH values. (b) UV-Vis spectra of rAgNAs at different pH values. (c) The corresponding maximum absorption peaks of rAgNAs in UV-Vis spectra (b).

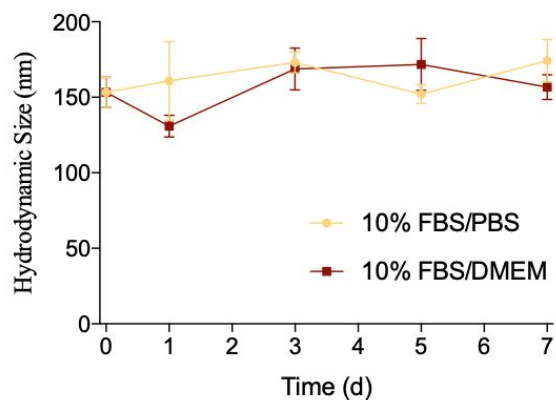


Figure S7. The hydrodynamic size measurement of rAgNAs in serum containing media (n = 3).

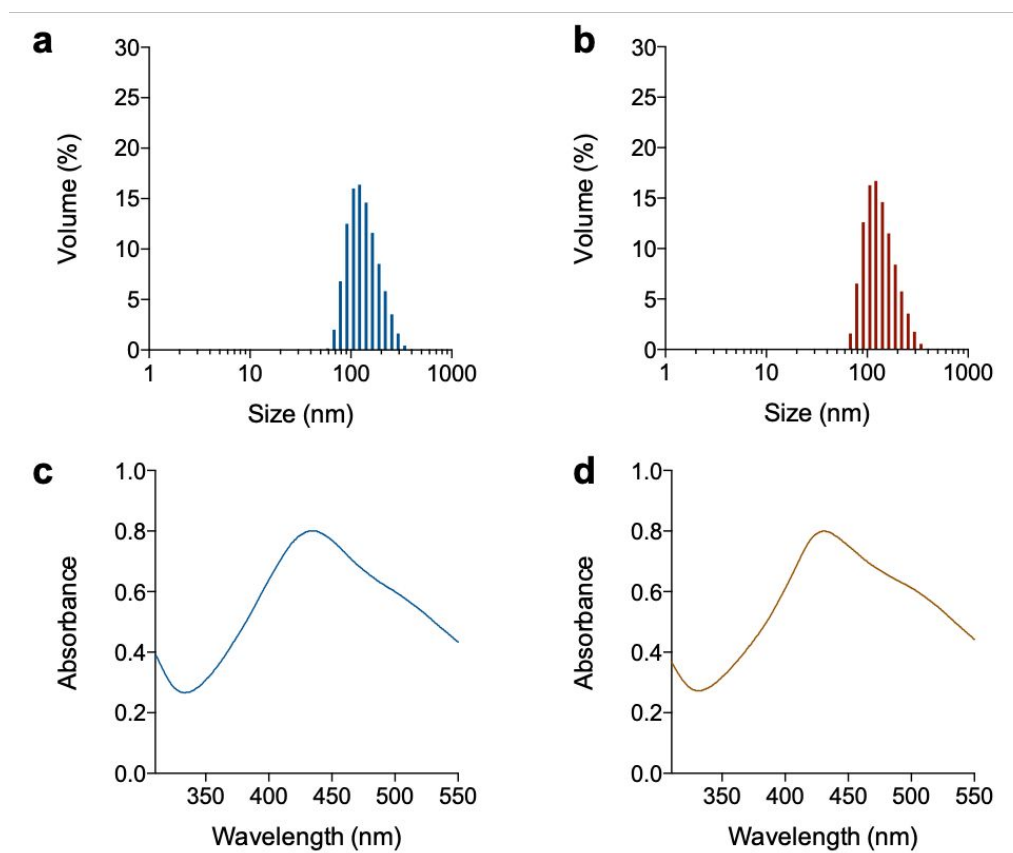


Figure S8. Characterization of uAgNAs. (a,b) Hydrodynamic size distribution profiles of uAgNAs at pH 7.4 (a) and pH 5.5 (b). (c,d) UV-vis spectra of uAgNAs at pH 7.4 (c) and pH 5.5 (d).

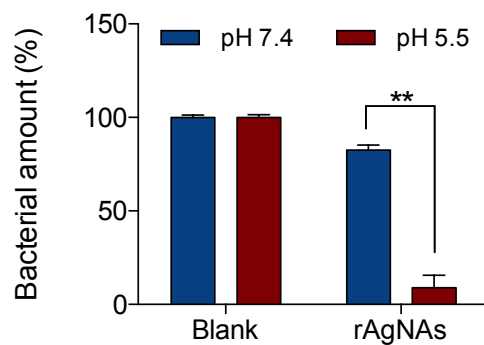


Figure S9. The relative growth quantity of planktonic MRSA co-cultured with rAgNAs in medium of different pH with concentration of $25 \mu\text{g mL}^{-1}$. $**P < 0.01$.

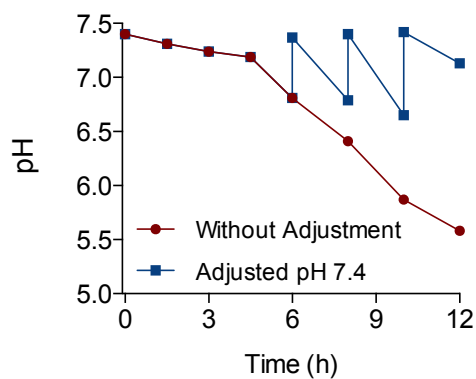


Figure S10. pH evaluation of the bacterial suspension during culture.

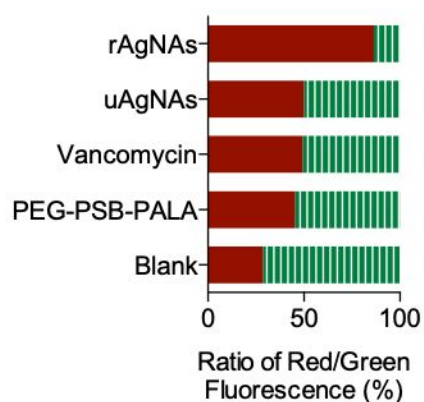


Figure S11. Quantitative statistics of the ratio of red/green fluorescence from the graphs of Syto green/PI staining of biofilm.

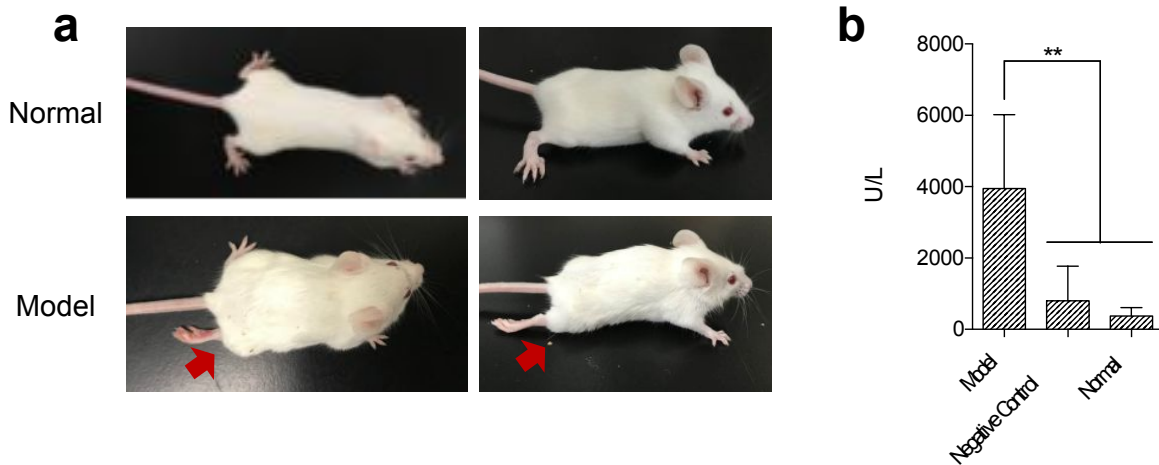


Figure S12. (a) Typical photographs of the infected model mice. (b) Levels of the serum creatine kinase after pyomyositis mice model establishment (n = 5). ** $P < 0.01$.

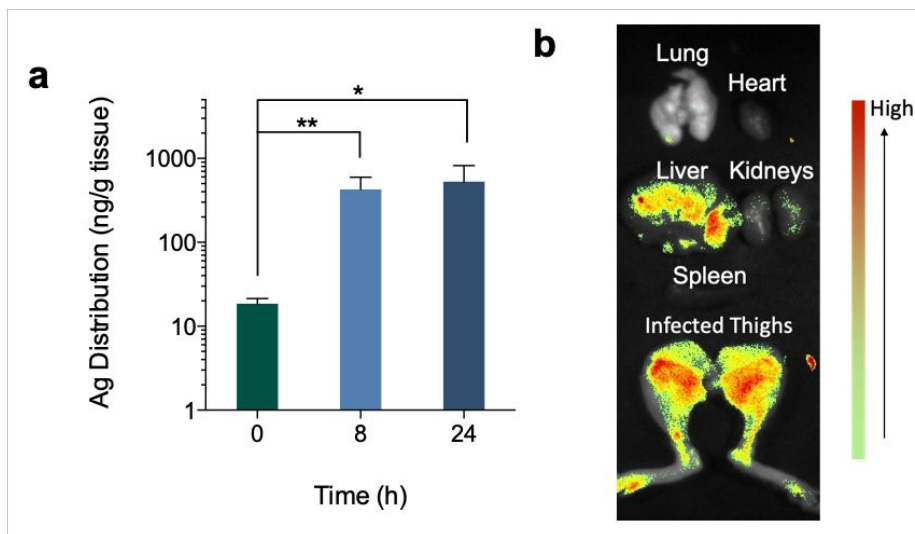


Figure S13. The biodistribution of rAgNAs. (a) Silver distribution in the infected muscle of pyomyositis model mice before and after rAgNAs treatment, as measured by ICP-MS. (b) *Ex vivo* fluorescence images of pyomyositis model mice post intravenous injection of RITC labeled rAgNAs.

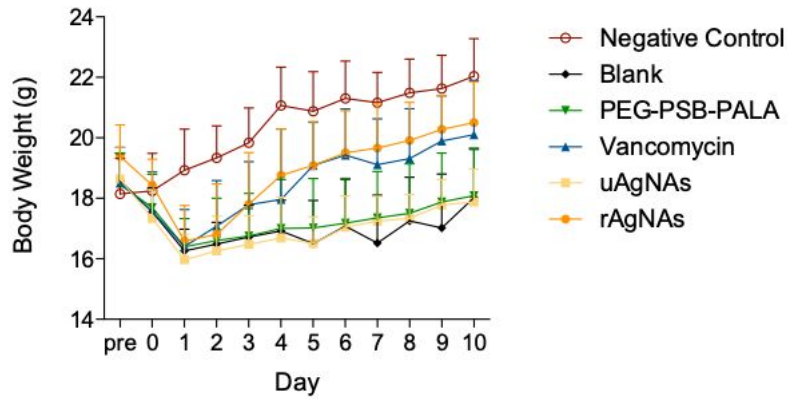


Figure S14. Curves of body weight of pyomyositis mice model in various groups during the treatments.

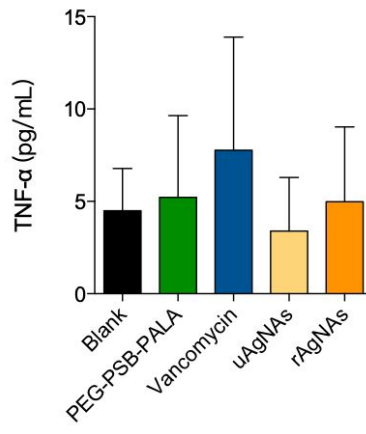


Figure S15. The serum level of TNF- α of the normal mice (n=5) with different treatments.

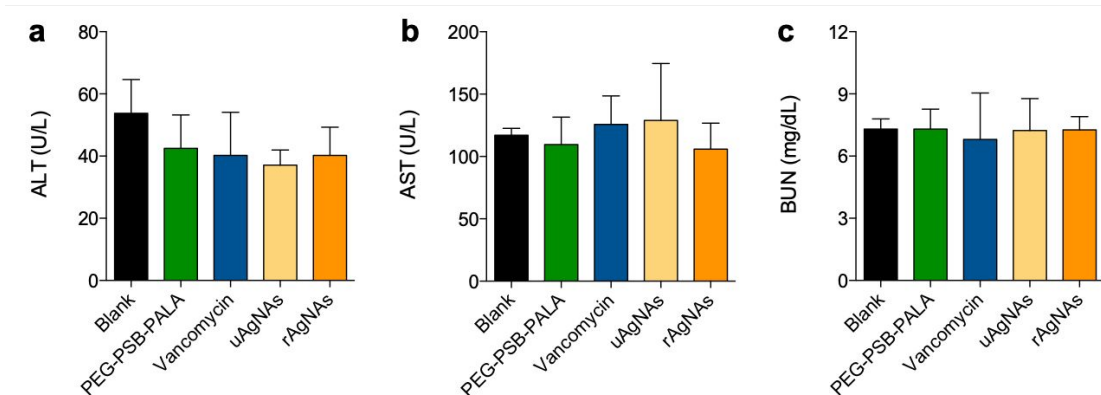


Figure S16. The levels of serum biochemicals including (a) ALT, (b) AST, and (c) BUN of the normal mice after different treatments (n=5).

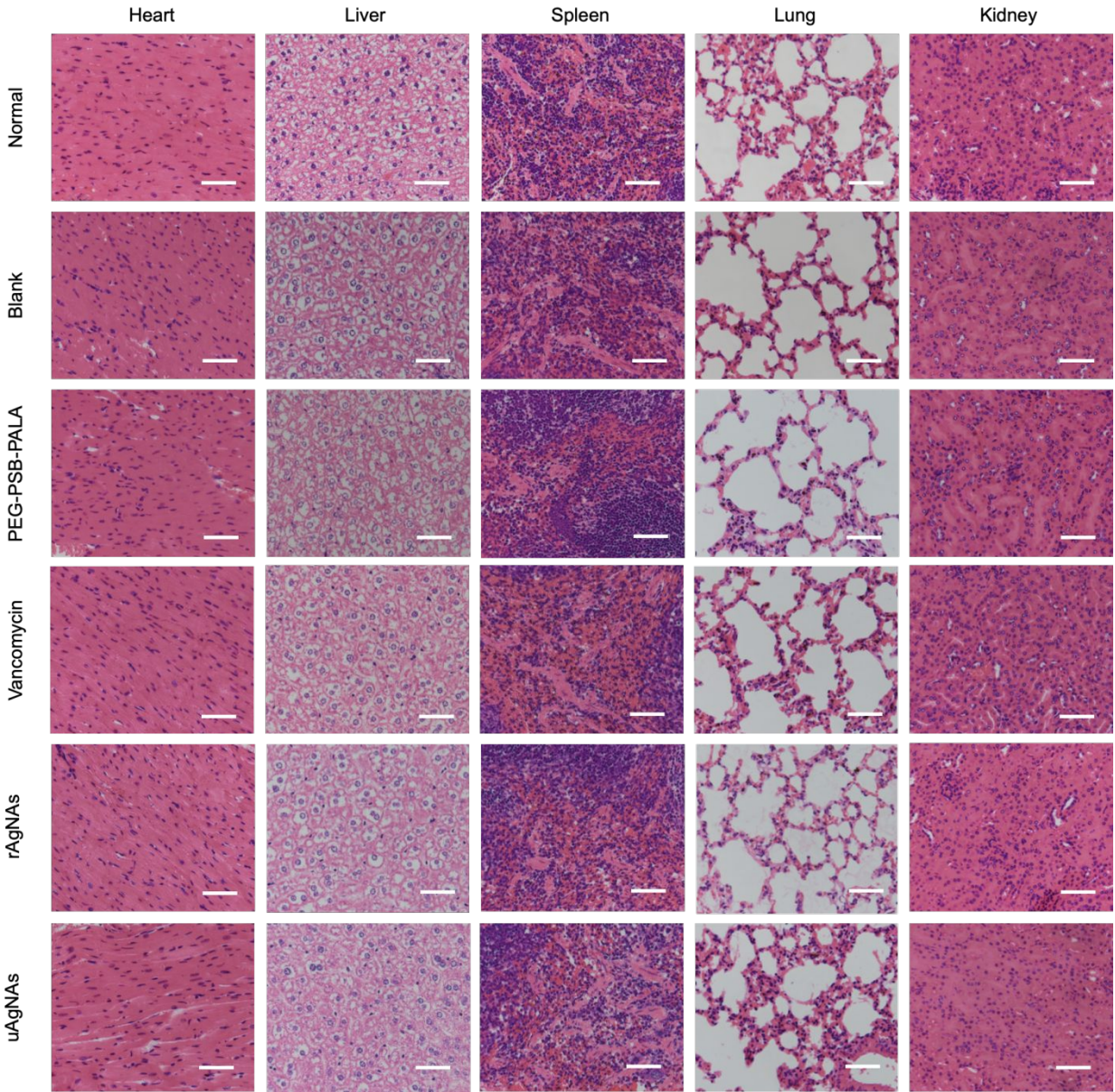


Figure S17. Hematoxylin and eosin (H&E) staining of main organs in various groups after being treated with therapeutic agents. Scale bar, 100 μ m.